

Does hepatobiliary phase sequence qualitatively outperform unenhanced T1-weighted imaging in assessment of the ablation margin 24 hours after thermal ablation of hepatocellular carcinomas?

Nobuyuki Takeyama,^{1,2} Sirachat Vidhyarkorn,^{2,3} Dong Jin Chung,^{2,4}
Surachate Siripongsakun,^{2,3} Hyun J. Kim,² David S. K. Lu,² Steven S. Raman²

¹Department of Radiology, Showa University Fujigaoka Hospital, Yokohama, Japan

²Department of Radiology, David Geffen School of Medicine at UCLA, 757 Westwood Blvd, Los Angeles, CA 90095, USA

³Department of Radiology, Chalubhorn Hospital, Bangkok, Thailand

⁴Department of Radiology, Catholic University of Korea, Seoul, South Korea

Abstract

Purpose: To retrospectively determine whether hepatobiliary phase (HBP) sequence outperforms unenhanced T1-weighted imaging (uT1wI) in distinguishing the ablation margin (AM) from hepatocellular carcinoma (HCC) 24 h after thermoablation.

Material and methods: Ninety-one patients [mean age, 65.7 years; 68 M/23F] with 138 HCCs (>6 months follow-up) underwent pre- and postablation gadoxetate disodium-enhanced MRI. AM showed a hyperintense middle zone (MZ) surrounding central hypo- or hyperintense HCCs on uT1wI, and an intermediate-intense MZ encompassing central hypo- or hyperintense HCCs during HBP. The visible AM was defined as persistent MZ around HCCs, which were demarcated from MZ, or peripherally band encompassing MZ, which were not demarcated from HCC. The indefinite AM was defined as no demarcating HCCs from MZ. The ability to distinguish AM from HCC was classified as visible or indefinite on axial (ax)-uT1wI, ax-HBP, coronal (cor)-HBP, and combined all images. To investigate the AM visibility during HBP, significance of differences upon comparison of ax-uT1wI with combined images was analyzed. Preablation liver-tumor contrast ratio (LTCR) on ax-uT1wI and ax-HBP sequence is compared between the visible and indefinite AM.

Results: The McNemar test demonstrated a significant increase ($p < 0.05$) in visible AM from ax-uT1wI (60), to ax-HBP (70), cor-HBP (79), and combined images (83). LTCR with visible AM was significantly higher than that with indefinite AM on ax-uT1wI (0.4 vs. 0.2, $p = 0.001$) and ax-HBP sequence (0.9 vs. 0.6, $p = 0.004$).

Conclusions: HBP sequence might have higher feasibility to distinguish AM from tumor than ax-uT1wI. The LTCR value in visible AM was higher than that in indefinite AM on both ax-uT1wI and ax-HBP sequences.

Key words: Hepatocellular carcinoma—Ablation margin—MRI—EOB—Hepatobiliary phase

In patients who had undergone percutaneous radiofrequency ablation (RFA) and microwave ablation (MWA) for local control of hepatocellular carcinoma (HCC), long-term imaging follow-up is necessary to detect tumor recurrence [1–3]. Imaging endpoints are critical to determine the treatment effectiveness because the ablation margin (AM) surrounding the lesion is an independent factor for local tumor progression (LTP)-free survival and for overall survival [4–6]. Although contrast-enhanced computed tomography (CT) is widely used, its efficacy to determine the AM is suboptimal not only due to its ionizing radiation but also because the ablation-induced hyperemic rim around the ablation zone may mimic residual tumor [7, 8]. Magnetic reso-

nance imaging (MRI) is a robust technique for liver imaging using a variety of techniques to provide a direct estimate of cell death. These include characteristic zones of ablation in animal studies and MRI-guided ablation studies [9–13].

In the acute phase within two days after thermal ablation, the ablation zone appears heterogeneously or peripherally hyperintense on unenhanced T1-weighted (T1w) imaging due to thermally induced dehydration and protein denaturation [1, 12–14]. Koda et al. have advocated that, in postablation MR images 2 and 7 h after RFA, unenhanced T1w imaging can demonstrate the AM surrounding central hypo- or hyperintense tumors, except in rare isointense target lesions [15]. On the other hand, Yoon et al. advocated gadoxetate disodium (Gd-EOB-DTPA)-enhanced MRI approximately 1.3 days after RFA to differentiate between the AM and tumor on portal venous phase images [16].

At our institution, all patients with liver thermal ablation for HCC undergo the EOB-enhanced MRI protocol including preablation, 24-h and 1-month postablation, and subsequently every 3 months thereafter. At interpretation of 24-h postablation MRI, we found that the signal intensity of the AM changed from hyperintensity on unenhanced T1w imaging to intermediate-intensity [16] during hepatobiliary phase (HBP); thus, we hypothesized that HBP could improve the conspicuity of AM in T1w iso-hyperintense tumor. In addition, coronal HBP images are expected to have higher feasibility to detect AM than axial unenhanced T1w images.

Therefore, the purpose of our study was to investigate the AM visibility during HBP 24 h after thermal ablation, in comparison of axial unenhanced T1w imaging with combined images (axial unenhanced T1w imaging + axial HBP + coronal HBP).

Materials and methods

Clinical features of patients

Institutional review board approval was obtained for a matched retrospective cohort study, and the requirements for informed consent were waived. The study was performed in compliance with the United States HIPAA.

From March 2010 to December 2013, 324 consecutive patients underwent the thermal ablation (RFA or MWA) for the treatment of HCC. Since March 2010, we have relied on EOB-enhanced MR imaging within 60 days prior to ablation, at 24 h and 1 month after ablation, and then for surveillance at serial 3 months intervals. Because only new lesions without prior focal therapy were evaluated to simplify assessment of the AM, the following patients were excluded: 36 with non-EOB gadolinium-enhanced MRI, 23 with CT only, 84 who underwent transcatheter arterial chemoembolization (TACE) or intra-arterial injection of Yttrium-90 microspheres as

neoadjuvant therapy prior to the thermal ablation, 61 with a follow-up period of less than 6 months, 17 who underwent repeated ablations including LTP ($n = 15$) and intrahepatic ablation along ablation tracts ($n = 2$), and 12 who were unable to perform breath-holding. Our study cohort comprised 138 HCCs in 91 patients [68 men and 23 women (age range, 36–87 years; mean age, 65.7 years)] who underwent preablation and 24-h postablation EOB-enhanced MR imaging (Fig. 1).

In 56 patients who underwent thermal ablation as the initial treatment, 80 HCCs were primary single or synchronous lesions. In 52 of 80 lesions, MR findings of them were not consistent with the Liver Imaging Reporting and Data System (LI-RADS) 5 criteria [17], including 8 lesions less than 10 mm in size. The US-guided biopsy confirmed the pathology of HCC ($n = 47$) and high-grade dysplastic nodules ($n = 5$). High-grade dysplastic nodules were treated as HCC due to their premalignant nature. In the other 28 lesions, MR imaging was in accordance with LI-RADS 5 criteria for HCC. In 35 patients with pathologically proven HCC who underwent the following treatment: RFA ($n = 14$), surgical resection ($n = 8$), RFA with surgical resection ($n = 7$), or TACE at other segments ($n = 6$), a total of 58 new lesions without abutting prior therapy met LI-RADS 5 criteria for HCC. They were defined as distant intrahepatic recurrence.

Of these 138 HCCs, 21 HCCs in 16 patients were found to have complete necrosis at transplantation during the follow-up period. Although 95 HCCs in 56 patients had no evidence of recurrence during the follow-up period, 22 HCCs in 19 patients had tumor recurrence (residual tumor and LTP). The presence or absence of LTP was decided by one of four radiologists who were not among the three radiologists who performed the quantitative and qualitative analyses. Residual tumor was most commonly caused by incomplete thermal ablation or local heat sink effect from larger vessels and was diagnosed as a nodular, eccentric, or circumferential lesion with moderate hyperintensity on T2-weighted (T2w) images with corresponding arterial phase enhancement and delayed phase washout [1–4]. LTP developed along the peripheral margin of the ablative lesion and was diagnosed as a nodular, eccentric, or circumferential lesion with arterial phase enhancement and delayed phase washout with gross enlargement relative to the ablated lesion and moderate hyperintensity on T2w images [1–4].

The mean follow-up period was 17.9 months (range, 6–45 months) and the mean interval between preablation examination and the procedure was 1.6 months (range, 0.3–4 months). The average largest diameter of tumors was 19.1 mm (range, 7–57 mm) on preablation MR images.

Table 1 summarizes the clinical and laboratory findings as the patients' baseline characteristics. With respect

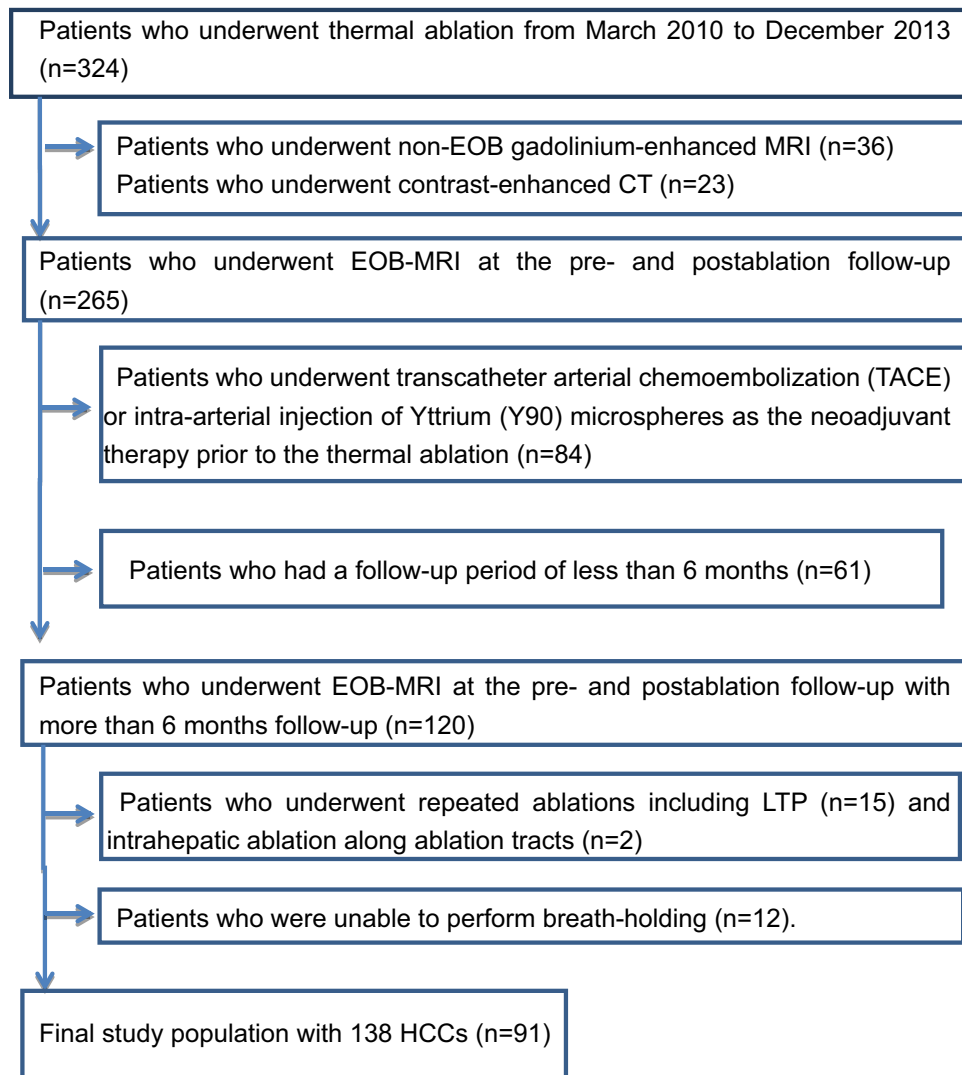


Fig. 1. Flow chart of inclusion and exclusion criteria of our study.

to tumor location, the Couinaud segmental anatomic classification was used, and the following three patterns were observed: subcapsular and subdiaphragmatic; abutting blood vessels within 3 mm from the first to third branches of the portal vein, hepatic vein, or inferior vena cava; and no relation to them.

The inclusion criteria for thermal ablation were as follows: (a) the target lesions were visualized by US and accessible via a percutaneous route; (b) the total tumor burden satisfied the Milan criteria (solitary tumor ≤ 5 cm, or three or fewer lesions none of which were > 3 cm in patients who were expected to complete treatment without being eligible for surgery; (c) no portal venous thrombosis and extrahepatic metastasis; (d) prothrombin time international normalized ratio [INR] < 1.7 ; (e) serum total bilirubin $< 3.0/\mu\text{L}$; and (f)

platelet count greater than $30 \times 10^3/\text{mL}$ without transfusion support.

Thermal ablation technique

All thermal ablations were performed under general anesthesia using both US and CT guidance. After selection of the target lesion, using real-time US guidance, the RF or MW probe was guided to the margin of the lesion. Multiple overlapping ablations were dependent on tumor size and tumor location. In cases that were not in accordance with LI-RADs 5 criteria, preablation biopsies were performed using 17/18-gage coaxial needles. In this study, HCCs were confirmed pathologically in 52 of 138 lesions. The ablation was terminated after both US and CT examinations showed an adequate estimated coagulation

Table 1. Clinical and laboratory findings as the patients' baseline characteristics

Characteristics of 91 patients of 138 HCCs	Value
Age (year) mean \pm SD (range)	65.7 \pm 10.0 (36–87)
Sex: male/female	68/23
Past history of RFA: yes/no	21/70
Past history of hepatectomy: yes/no	15/76
Child-pugh score: A/B/C	114/24/0
Etiology Alcoholism/HBV/HCV/HBV + HCV/NASH/AIH/unknown/hepatic adenoma	6/26/43/2/4/1/7/1
Platelet count ($\times 10^3/\mu\text{L}$) mean \pm SD (range)	104.3 \pm 56.9 (30–279)
Prothrombin time with international normalized ratio [INR] mean \pm SD (range)	1.1 \pm 0.2 (1.0–1.8)
Serum Bilirubin (mg/dL) mean \pm SD (range)	1.1 \pm 0.6 (0.3–3)
Serum Albumin (g/dL) mean \pm SD (range)	3.8 \pm 0.6 (2.1–4.9)
Serum AFP (ng/mL) mean \pm SD (range)	113.9 \pm 542.9 (0.8–5650)
Follow-up (months) mean \pm SD (range)	17.9 \pm 9.8 (6–45)
Preablation tumor size (mm) mean \pm SD (range)	19.1 \pm 8.6 (7–57)
Tumor status primary synchronous single/two/three/four	60/20/19/4
Intrahepatic distant metastasis single/two/three/four	21/11/0/3
Tumor location Abutting vessels / Subcapsular or diaphragmatic / others	72/11/56
Segment I/II/III/IV/V/VI/VII/VIII	3/11/16/17/15/31/13/33

zone; however, if the coagulation zone insufficiently covered the tumor after the contrast-enhanced CT, additional ablation was performed. Electrode and probe track ablation was also performed to minimize postprocedural bleeding and tumor seeding along the track.

Out of 113 RFA procedures, 17-gage cooled-tip electrodes with internally advancing single electrodes ($n = 27$), double electrodes ($n = 72$), triple electrodes ($n = 2$), and cluster electrodes ($n = 12$) were used. Each ablation session was performed with power increased from 80 to 160 W for 4–16 min. MWA procedures were performed using a 16- or 17-gaged internal probe. For 25 MWA procedures, single ($n = 9$) or double ($n = 16$) probes were used. Each ablation session was performed with power increased from 40 to 140 W for 2–16 minutes.

All procedures were performed by one of four radiologists with up to 15 years of experience in liver ablation.

MRI protocol

The preablation MRI examinations for outpatients were performed on either a 1.5-T system (Avanto, or Sonata, Siemens Healthcare; and Signa HDxt, GE Healthcare) or a 3-T system (Skyra, Verio, or Trio, Siemens Healthcare) using a phased-array torso coil. The postablation MRI examinations for inpatients were conducted on the Avanto ($n = 120$) or Trio ($n = 18$).

The standard protocol of MR sequences includes T2w half-Fourier acquisition single-shot turbo spin echo (HASTE) or single-shot first spin echo (SSFSE) sequence in coronal and axial planes, 2D gradient-echo in- and opposed-phase imaging in the axial plane, and a diffusion-weighted axial echo planar imaging sequence in the axial plane. Here, unenhanced and contrast-enhanced T1w series were obtained with the use of 3D gradient-echo sequences (VIBE or LAVA) with fat saturation using the

following parameters: TR range, 2.88–5.41 ms; TE range, 1.2–2.38 ms; flip angle, 10°–12°; section thickness range; 2.5–5 mm; and matrix range, 256 \times 96–180, 320 \times 156–264, or 384 \times 144–235 in both axial and coronal phases. FOV of each sequence was 38–44 cm. The dynamic contrast-enhanced images in the axial plane were obtained at the arterial phase, portal venous phase (70–90 s), and late phase (180 s) after IV bolus injection of 10 mL of gadopentetate disodium (Eovist, Bayer Schering Pharma). The arterial phase was started with a 5 s delay from the contrast visualization of the abdominal aorta using the care bolus technique. FOV of each phase ranged from 38 to 44 cm. In addition, HBP series were obtained at 18 and 20 min in axial and coronal planes. In cases of suboptimal image quality, for example, due to motion artifacts during HBP, repeated acquisitions were performed in both axial and coronal phases. The bolus was injected at a rate of 1–2 mL/s and flushed with saline.

Qualitative analysis

All MR imaging studies were retrospectively assessed by two abdominal radiologists, with 20 years (C.J.I.) and 10 years (V.S.) of experience of MRI interpretation of the liver, who knew the diagnosis of HCC and information about tumor location, but were unaware of laboratory data, other imaging findings, and final results in terms of whether residual tumor and LTP occurred during the follow-up period. Reviewers first reviewed the preablation imaging of the tumor and then postablation scan on unenhanced T1w, HBP, and combined images (Fig. 3). The qualitative analysis was to evaluate the AM visibility classified as visible or indefinite [15, 18]. After the AM visibility was assessed, the interobserver comparison was analyzed on axial unenhanced T1w imaging, axial HBP, and coronal HBP. In cases, which two readers had different opinions, discrepancies were resolved by discussion in order to reach a consensus. Next,

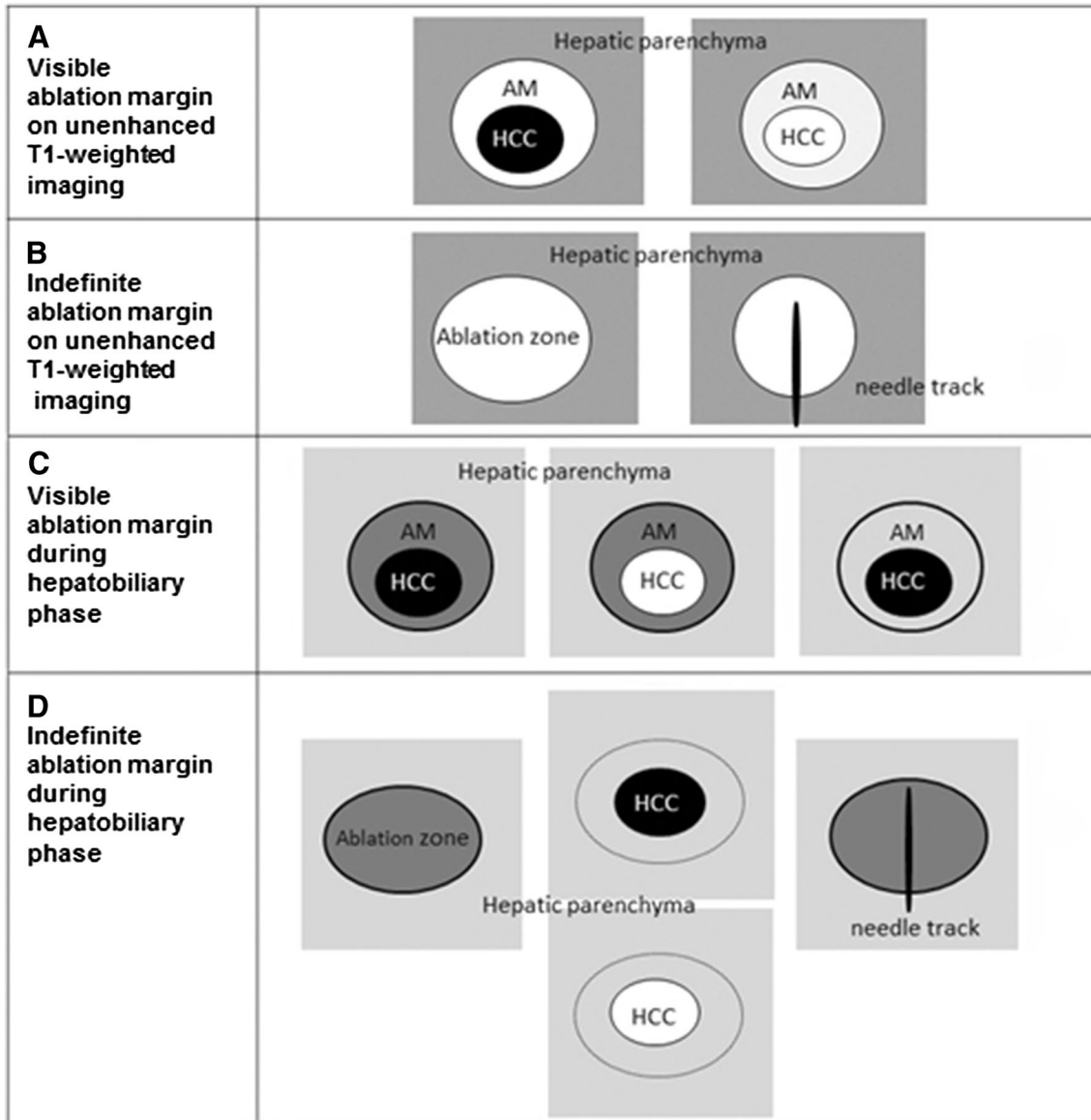


Fig. 2. Schematic interpretation of postablation unenhanced T1-weighted and hepatobiliary phase images. On the unenhanced T1-weighted image, visible AM (**A**) was defined as a central hypo- or hyperintense tumor circumscribed by a broad hyperintense middle zone, and indefinite AM (**B**) was defined by an indistinct or poorly visualized central hypo- or hyperintense tumor, circumscribed by a broad hyperintense *middle zone*, and needle track within the broad hyperintense *middle zone*. During the hepatobiliary phase, visible AM (**C**) was de-

defined as central hypo- or hyperintense tumor circumscribed by a broad intermediate-intensity *middle zone* with a marginal hypointense band, or a central hypointense tumor with a marginal hypointense band when the *middle zone* showed similar intensity to be hepatic parenchyma. Indefinite AM (**D**) was assigned when the central lesion could not be easily distinguished from the ablated zone and the *middle zone* demonstrated the same intensity as hepatic parenchyma, and needle track was within the broad intermediate-intense *middle zone*.

reviewers asked the AM status (AM plus, AM zero, or AM minus). Combined images were analyzed in patients whose AM could be analyzed visually [18]. After classification of the AM status was finished, interobserver comparison was assessed. Then, discrepancies between the two reviewers were resolved by discussion in order to reach a consensus.

With regard to the AM visibility, the size and shape of the central lesion could be distinguished as similar or slightly collapsed, compared to those of the index lesion on preablation MR imaging. In both visible and indefinite cases, the treated lesion was surrounded by an ablation zone. The visible AM was defined as the presence of a persistent middle zone around the treated tu-

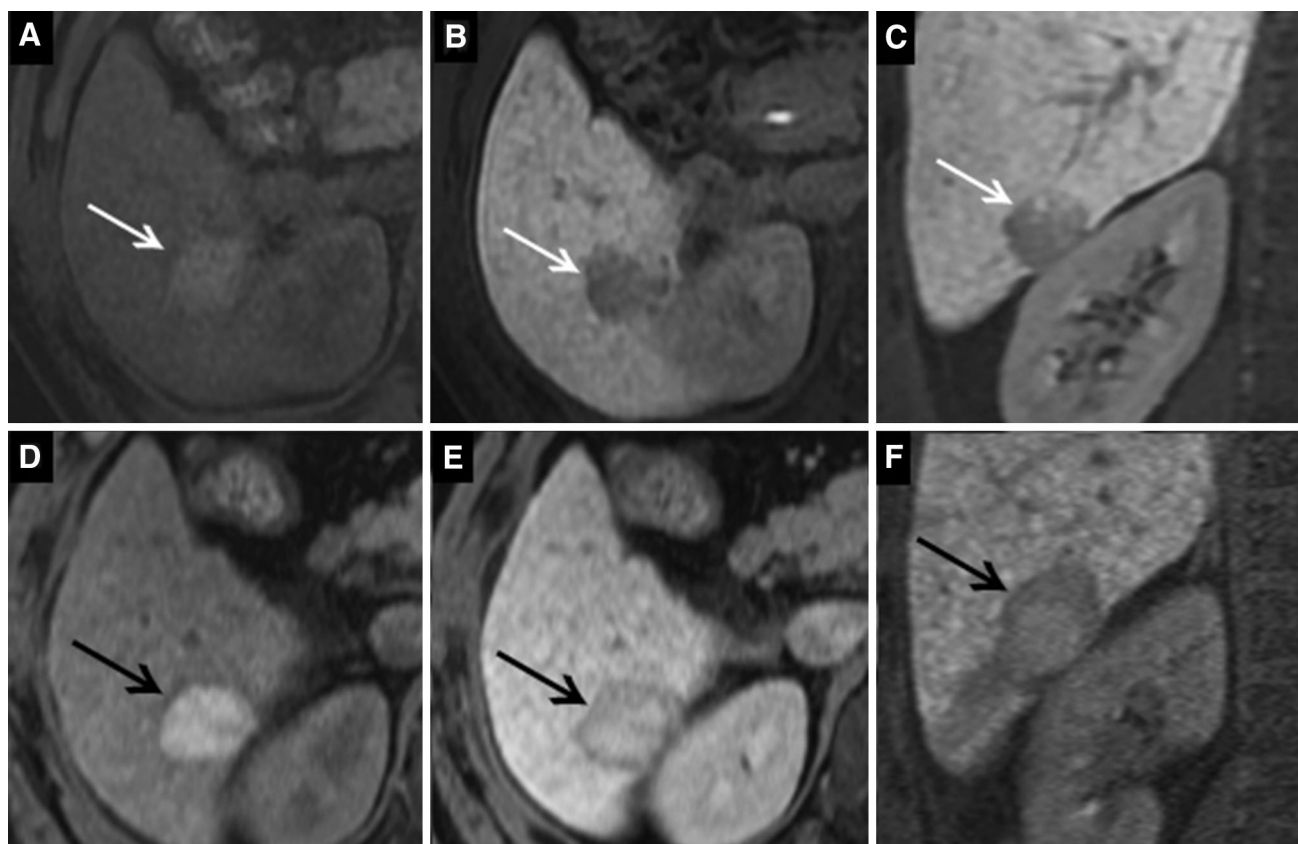


Fig. 3. Images in a 50-year-old man with well-differentiated hepatocellular carcinoma. At preablation MR imaging, the axial unenhanced T1-weighted image (**A**) shows hyperintense tumor (*white arrow*), and axial (**B**) and coronal (**C**) hepatobiliary phase images demonstrate hypointense tumor (*white arrows*). Tumor size is 26 mm, and TLCR on axial unenhanced T1-weighted and HBP imaging are 0.19 and 2.04. After radiofrequency ablation for tumor, axial unenhanced T1-weighted imaging (**D**) does not distinguish from a broad

hyperintense ablation margin from the central hyperintense tumor (*black arrow*). The ablation margin is classified as indefinite. Axial (**E**) and coronal (**F**) hepatobiliary phase images show central hyperintense tumor surrounded by a broad intermediate-intense ablation margin (*black arrows*). The ablation margin is classified as visible. Using combined images, the status of the ablation margin is AM zero. During 8 months follow-up, there is no evidence of local tumor progression.

hyperintensity on unenhanced T1w imaging and as intermediate-intensity during HBP: AM plus, in which the AM was completely surrounded the tumor; AM zero, in which the AM was partially discontinuous, without protrusion of the tumor beyond the border of the ablative zone; and AM minus, in which the AM was partially discontinuous, with protrusion of the tumor (Figs. 4, 5). The two reviewers were free to use processing tools, such as windowing, gradation adjustment, or magnification, and to scroll the MRI examinations. Readings were performed on a PACS-integrated workstation (Centricity RA 1000, GE Healthcare) with a 21.5-inch display and a resolution of 1920×1080 pixels.

mor, demarcating it from the AM. The indefinite AM was defined as no demarcating tumor from the AM, including only the needle track. On axial HBP sequence, the visible AM was defined as a central tumor circumscribed by a broad intermediate-intense middle zone, or a central tumor with a marginal hypointense band when the middle zone showed similar intensity to hepatic parenchyma (Fig. 2C). Indefinite AM was defined as a central lesion that could not be easily distinguished from the ablated zone, the middle zone demonstrated the same intensity as hepatic parenchyma, or including only the needle track (Fig. 2D). On combined image review, the visible AM met the visible criteria on either unenhanced T1w or HBP images, and the indefinite AM met indefinite criteria on either unenhanced T1w or HBP images (Fig. 3).

The AM status was classified as one of 3 types [18] in patients whose AM could be analyzed visually as

hyperintensity on unenhanced T1w imaging and as intermediate-intensity during HBP: AM plus, in which the AM was completely surrounded the tumor; AM zero, in which the AM was partially discontinuous, without protrusion of the tumor beyond the border of the ablative zone; and AM minus, in which the AM was partially discontinuous, with protrusion of the tumor (Figs. 4, 5).

The two reviewers were free to use processing tools, such as windowing, gradation adjustment, or magnification, and to scroll the MRI examinations. Readings were performed on a PACS-integrated workstation (Centricity RA 1000, GE Healthcare) with a 21.5-inch display and a resolution of 1920×1080 pixels.

Quantitative assessment

One experienced radiologist (N.T) with 12 years of clinical experience in liver MRI measured signal intensity

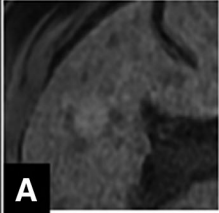
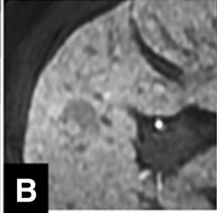
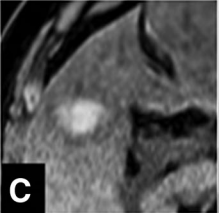
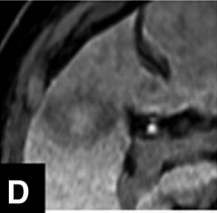

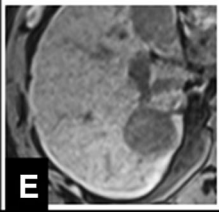
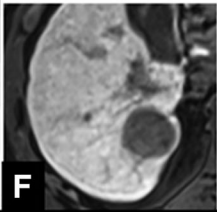
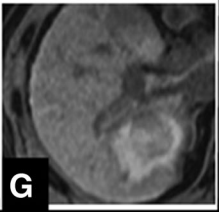
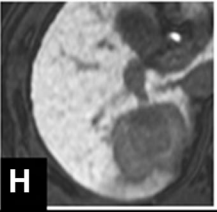

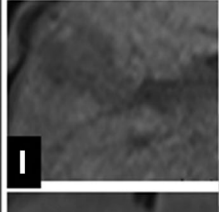
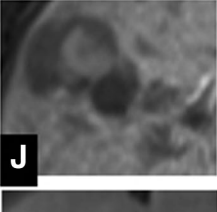
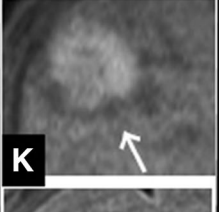
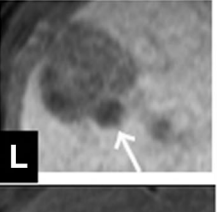
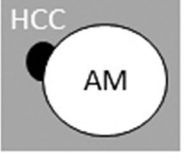




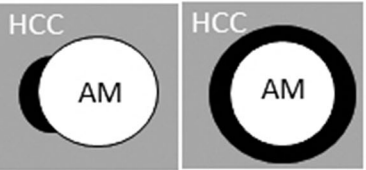
Preablation unenhanced T1-weighted imaging	Preablation hepatobiliary phase	Postablation Unenhanced T1-weighted imaging	Postablation Hepatobiliary phase	Grade of AM status
				AM (+) 
				AM (zero) 
				AM (-) 
				

Fig. 4. Grade of ablation margin status. Status of ablation margin (AM) was categorized as the following three types: AM (+), AM (zero), and AM (-). Schema shows successful ablation and subsequent involution of the ablation zone. At preablation MR imaging, the axial unenhanced T1-weighted image (A) shows an iso-hyperintense tumor, and the hepatobiliary phase image (B) demonstrates a hypointense tumor, including an isointense component. After radiofrequency ablation for tumor, axial unenhanced T1-weighted imaging (C) shows a central hyperintense tumor and a broad ablation margin with slightly hyperintensity, and the axial hepatobiliary phase image (D) demonstrates a central hyperintense tumor encompassed by a broad intermediate-intense ablation margin as AM (+). Marginal hypointense band could not be visualized in the plane. Schema shows successful ablation and subsequent involution of the ablation zone. At preablation MR imaging, the axial unenhanced T1-weighted image (E) and hepatobiliary phase (F) show a hypointense tumor. After radiofrequency ablation for the tumor, axial unenhanced T1-weighted imaging (G) shows a central hypointense tumor and a broad hyperintense ablation margin as AM zero, and axial

hepatobiliary phase image (H) demonstrates central hypointense tumor, broad intermediate-intense ablation margin, and marginal thin hypointense band. Schema shows incomplete ablation, with a nodular remnant of tumor tissue at the margin of the ablation zone. At preablation, the axial unenhanced T1-weighted (I) and hepatobiliary phase (J) images show hypointense nodules. After radiofrequency ablation for tumor, axial unenhanced T1-weighted imaging (K) shows peripheral slightly hypointense nodular tumor (arrow) against the hyperintense ablation zone, and hepatobiliary phase image (L) demonstrates a nodular hypointense residual tumor (arrow). Schema shows incomplete ablation, with a crescent-shaped remnant of tumor tissue at the margin of the ablation zone. At preablation, the axial unenhanced T1-weighted image (M) and axial hepatobiliary phase (N) show a hypointense tumor. After radiofrequency ablation for the tumor, axial unenhanced T1-weighted imaging (O) shows a subcapsular crescentic hypointense residual tumor (arrow) against the hyperintense ablation zone, and axial hepatobiliary phase image (P) shows a crescentic hypointense residual tumor (arrow).

(SI) for HCC, the adjacent liver parenchyma, and paraspinal muscle. The tumor-liver contrast ratio (TLCR) was calculated from measurements of SI on axial unen-

hanced T1w and HBP images as follows: $|SI \text{ of tumor} - SI \text{ of liver parenchyma}| / SI \text{ of paraspinal muscle}$. The region of interest (ROI) for HCC, the adjacent liver par-

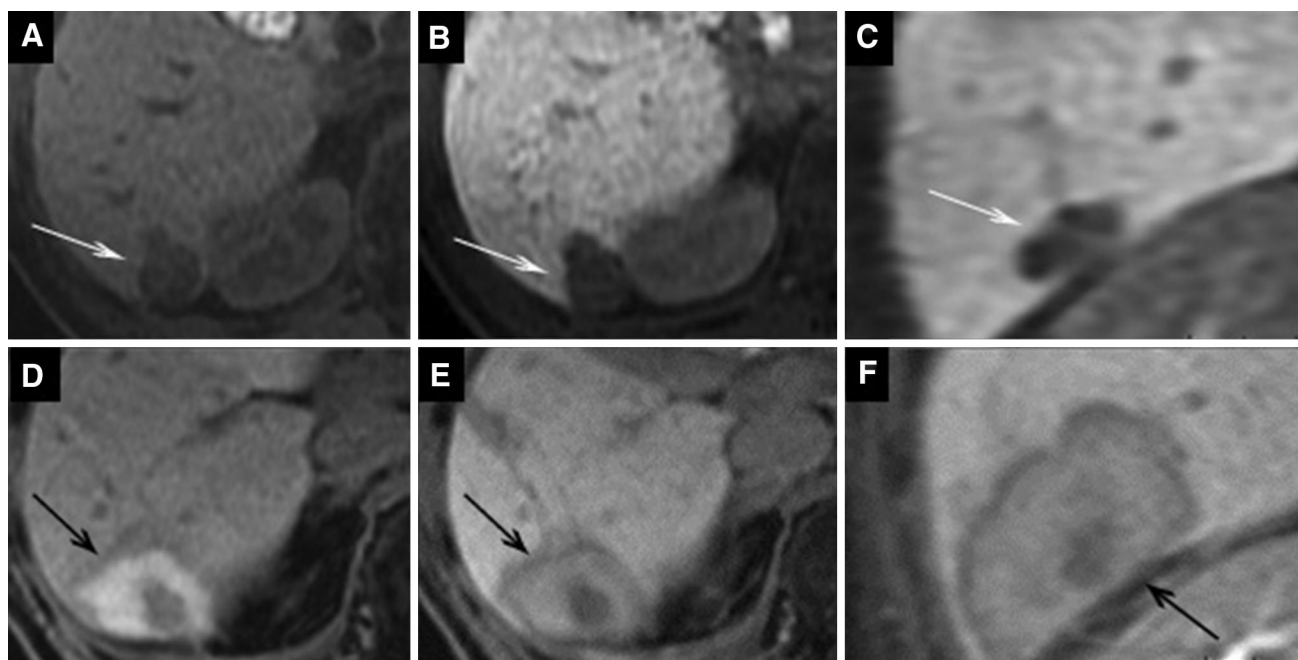


Fig. 5. Images in a 80-year-old man with moderately differentiated hepatocellular carcinoma. At preablation MR imaging, the axial unenhanced T1-weighted image (**A**) shows a hypointense tumor (*white arrow*), and axial (**B**) and coronal (**C**) hepatobiliary phase images show a hypointense tumor (*white arrows*). Tumor size is 23 mm, and TLCR on axial unenhanced T1-weighted and HBP imaging are 0.65 and 1.94. After radiofrequency ablation for the tumor, axial unenhanced T1-weighted imaging (**D**) shows a collapsed central

enchyma, and paraspinous muscle were drawn on the same axial image. The size of ROI for each region was at least 2 cm². The ROI of HCC was placed at the highest signal with exclusion of vessels. The ROI of the liver parenchyma was placed at four points surrounding HCC, and that of paraspinous muscle was at the bilateral psoas muscle. The SI of the adjacent liver parenchyma and paraspinous muscle were calculated as an average value.

Statistical analysis

All data are shown as mean values \pm standard deviations. Statistical analysis was performed using Stata version 12.0 (Stata Corporation, College Station, TX). The numbers and percentages of patients to evaluate the AM visibility (visible and indefinite) on postablation axial unenhanced T1w imaging, axial HBP, coronal HBP, and combined images were compared using the McNemar test. The relationships between tumor signal (hypo- or iso-hyperintensity) on preablation unenhanced T1w imaging and AM visibility (visible or indefinite) on postablation axial unenhanced T1w imaging, axial HBP, coronal HBP, and combined images were compared using the McNemar test, and the relationships between tumor signal (hypo- or iso-hyperintensity) during pre-

hypointense tumor and a broad hyperintense ablation margin (*black arrow*). This ablation margin is classified as visible. Axial (**E**) and coronal (**F**) hepatobiliary phase images show a central hypointense tumor with an intermediate-intensity ablation margin (*black arrows*). This ablation margin is classified as visible. Using combined images, the status of the ablation margin is AM plus. During 34 months follow-up, there is no evidence of local tumor progression.

ablation HBP and AM visibility (visible or indefinite) on postablation axial unenhanced T1w imaging, axial HBP, coronal HBP, and combined images were also compared using the McNemar test. The relationships of visibility and status of AM and the incidence of recurrence were analyzed using the Chi-square test in the stable group and Fisher exact test in the recurrence group.

Interobserver agreement to evaluate the AM visibility on axial unenhanced T1w imaging, axial HBP, and coronal HBP were evaluated using the Cohen k coefficient, respectively. Interobserver agreement to investigate the AM status using combined images was analyzed using the Cohen weighted-kappa coefficient. The k values were interpreted as poor for k less than 0.20; fair, k of 0.21–0.40; moderate, k of 0.40–0.60; good, k of 0.61–0.80; and very good, k of 0.81–1.00. Probability values less than 0.05 were considered significant.

Comparison of TLCR between the visible and indefinite AM on axial unenhanced T1w and axial HBP images was analyzed, using unpaired t test.

Results

Table 2 shows that the numbers and percentages of the 138 ablation zones with visible AM on axial unenhanced T1w

imaging, axial HBP, coronal HBP, and combined images. There were significant increases in ablation zones with visible AM from axial unenhanced T1w imaging, to axial HBP ($p = 0.041$), coronal HBP ($p < 0.01$), and combined images ($p < 0.01$), respectively. Table 3 shows that 82 (59.4%) HCCs were hypointense and 56 (40.6%) HCCs were iso-hyperintense on preablation unenhanced T1w images. In 82 hypointense HCCs, there were significant increases in ablation zones with visible AM from axial unenhanced T1w imaging, to coronal HBP ($p = 0.013$), and combined images ($p < 0.01$). In 56 iso-hyperintense HCCs, there were significant increases in ablation zones with visible AM from axial unenhanced T1w imaging, to coronal HBP ($p = 0.040$) and combined images

($p = 0.012$). In 126 hypointense HCCs during HBP, there were significant increases (Table 4) in ablation zones with visible AM from axial unenhanced T1w imaging, to axial HBP ($p = 0.041$), coronal HBP ($p < 0.01$), and combined images ($p < 0.01$). In 12 iso-hyperintense HCCs during HBP, the numbers of ablation zones with visible AM on axial unenhanced T1w imaging, axial HBP, coronal HBP, and combined images did not significantly increase. Table 5 shows the relationship between AM visibility and outcome during the follow-up period. Combined images were superior to axial unenhanced T1w imaging in AM visibility in the stable ($p < 0.001$) group and recurrence group ($p = 0.002$). When combined images were reviewed in comparison to unenhanced T1w

Table 2. Comparison of the AM visibility on postablation axial unenhanced T1w imaging with other images in 138 HCCs

Postablation images	The AM visibility		
	Visible AM (AM+, AM0, and AM-)	Indefinite AM including needle track	<i>p</i> value
Axial unenhanced T1w imaging	60 (43.5)	78 (56.5)	
Axial HBP	70 (50.7)	68 (49.3)	$p = 0.041$
Coronal HBP	79 (57.2)	59 (42.8)	$p < 0.01$
Combined images (axial unenhanced T1w imaging + axial HBP + coronal HBP)	83 (60.1)	55 (39.9)	$p < 0.01$

Data are numbers of HCCs, with the percentage in parentheses
 AM ablation margin, T1w T1-weighted, HBP hepatobiliary phase

Table 3. Relationship between signal intensity of tumors on preablation unenhanced T1w imaging and the AM visibility on postablation axial HBP, coronal HBP, and combined images, compared with those on axial unenhanced T1w imaging

Postablation image	Preablation image					
	Hypointense tumors ($n = 82$) on unenhanced T1w imaging			Iso-hyperintense tumors ($n = 56$) on unenhanced T1w imaging		
	AM visible	AM indefinite	<i>p</i> value	AM visible	AM indefinite	<i>p</i> value
The AM visibility						
Axial unenhanced T1w imaging	51	31		9	47	
Axial HBP	55	27	$p = 0.338$	15	41	$p = 0.07$
Coronal HBP	61	21	$p = 0.013$	18	38	$p = 0.040$
Combined images (axial unenhanced T1w imaging + axial HBP + coronal HBP)	64	18	$p < 0.01$	19	37	$p = 0.012$

Data are numbers of HCCs
 AM ablation margin, T1w T1-weighted, HBP hepatobiliary phase

Table 4. Relationship of signal intensity of tumors on preablation HBP images and the AM visibility on postablation axial HBP, coronal HBP, and combined images, compared with those on axial unenhanced T1w imaging

Postablation	Preablation image					
	Hypointense tumors ($n = 126$) on preablation HBP images			Iso-hyperintense tumors ($n = 12$) on preablation HBP images		
	AM visible	AM indefinite	<i>p</i> value	AM visible	AM indefinite	<i>p</i> value
The AM visibility						
Axial unenhanced T1w imaging	57	69		3	9	
Axial HBP	67	59	$p = 0.041$	3	9	$p = 1.00$
Coronal HBP	75	51	$p < 0.01$	4	8	$p = 1.00$
Combined images (axial unenhanced T1w imaging + axial HBP + coronal HBP)	79	47	$p < 0.01$	4	8	$p = 1.00$

Data are numbers of HCCs
 AM ablation margin, T1w T1-weighted, HBP hepatobiliary phase

Table 5. Comparison between axial unenhanced T1w imaging and combined images (axial unenhanced T1w imaging + axial HBP + coronal HBP) in visibility and status of AM in the stable and recurrence groups

	Visibility and grades of AM					<i>p</i> value
	Visible AM		AM–	Indefinite AM		
	AM+	AM0		Indefinite	Needle track	
Stable group (<i>n</i> = 116)						<i>p</i> < 0.01
Axial unenhanced T1w imaging	29	21	0	61	5	
Combined images	54	14	0	43	5	
Recurrence group (<i>n</i> = 22)						<i>p</i> = 0.002
Axial unenhanced T1w imaging	5	1	4	12	0	
Combined images	1	3	11	7	0	

Data are numbers of HCCs

AM ablation margin, T1w T1-weighted, HBP hepatobiliary phase

imaging, 7 of 21 visible AM (AM zero) and 18 of 61 indefinite AM were changed to visible AM (AM plus) in the stable group (*n* = 116). In the recurrence group, 2 of 5 visible AM (AM plus) and 5 of 12 indefinite AM were changed to visible AM (AM minus), and 2 of 5 visible AM (AM plus) were changed to visible AM (AM zero).

Agreement levels about the AM visibility in 138 patients on axial unenhanced T1w imaging, axial HBP, and coronal HBP were good ($k = 0.779$; 95% confidence interval: 0.674, 0.885), good ($k = 0.797$; 95% confidence interval: 0.696, 0.898), and very good ($k = 0.825$; 95% confidence interval: 0.730, 0.919), respectively. The agreement for analysis of the AM status in 83 patients using combined images was good ($k = 0.764$; 95% confidence interval: 0.594, 0.868).

The averaged TLCR on axial unenhanced T1w imaging was 0.3 ± 0.3 , ranging from 0 to 1.22, and that on axial HBP sequence was 0.8 ± 0.6 , ranging from 0.01 to 3.31. On axial unenhanced T1w images (Fig. 8A), TLCR (0.4 ± 0.2) in the visible AM (*n* = 60) was significantly higher ($p = 0.001$) than that (0.2 ± 0.3) in indefinite AM (*n* = 78). On axial HBP sequences (Fig. 8B), TLCR (0.9 ± 0.6) in the visible AM (*n* = 70) was significantly higher ($p = 0.002$) than that (0.6 ± 0.5) in the indefinite AM (*n* = 68).

Discussion

To our knowledge, there is no report to compare unenhanced T1w and HBP images on Gd-EOB-DTPA-enhanced MRI 24 h after ablation, although Ringe et al. [19] describes that additional Gd-BOPTA-MRI 24 h after CT-guided ablation seems of limited value regarding prognosis of LTP, especially with regard to evaluation of AM.

On postablation unenhanced T1w imaging, preablation hypo- and hyperintense tumors can be identified within hyperintense AM due to the SI differences between AM and tumor, or AM and hepatic parenchyma, because the hyperintense ablative zone includes coagulation necrosis, hemorrhage product, and dehydration [2].

Regarding AM visibility, 51 (62.2%) of 82 hypointense tumors on unenhanced T1w images 24 h after ablation could be distinguished from AM. This result is worse than data published by Koda et al. that 12 of 14 (85.8%) hypointense tumors could be visualized 7 h after ablation [15]. It was considered that scan timing after procedures might have caused this difference because 4-h postablation unenhanced T1w images enabled visualization of AM, but 24-h postablation images did not [15]. We believe that the SI of a tumor could gradually increase after thermal ablation with shrinkage due to tissue loss, until hemorrhage and coagulation necrosis would completely replace the ablation zone. Considering the SI of the ablation zone on both unenhanced T1w and T2w images varies over time according to the stage of hemorrhage, the type of necrosis [20], or the host response [7], unenhanced T1w imaging 7 h after the ablation has higher utility than HBP sequences at 24 h. However, scan timing of MRI within 24 h after termination may optimal to identify tumor within the ablation zone, because patients underwent MR examination 24 h after awaking from general anesthesia.

This hypothesis might resolve the inability to distinguish AM from isointense tumor because if tumor shows the same intensity as hepatic parenchyma on preablation unenhanced T1w imaging [15], postablation unenhanced T1w imaging cannot provide the SI difference between ablated isointense tumor and AM.

Although the preablation TLCR in visible AM was significantly higher than that in indefinite AM on unenhanced T1w and HBP imaging, both figures of box and whisker plot (Fig. 8A, B) shows too much overlap to establish a threshold value to predict whether the AM will be visible or not. Although the reablation TLCR value might be a factor that creates contrast between the AM and tumor after ablation, we consider that other factors might affect this contrast, such as tumor diameter, ablation procedure time, number of electrodes, and background liver function to take up GD-EOB DTPA through the organic anion transporting polypeptide within the hepatocyte membrane.

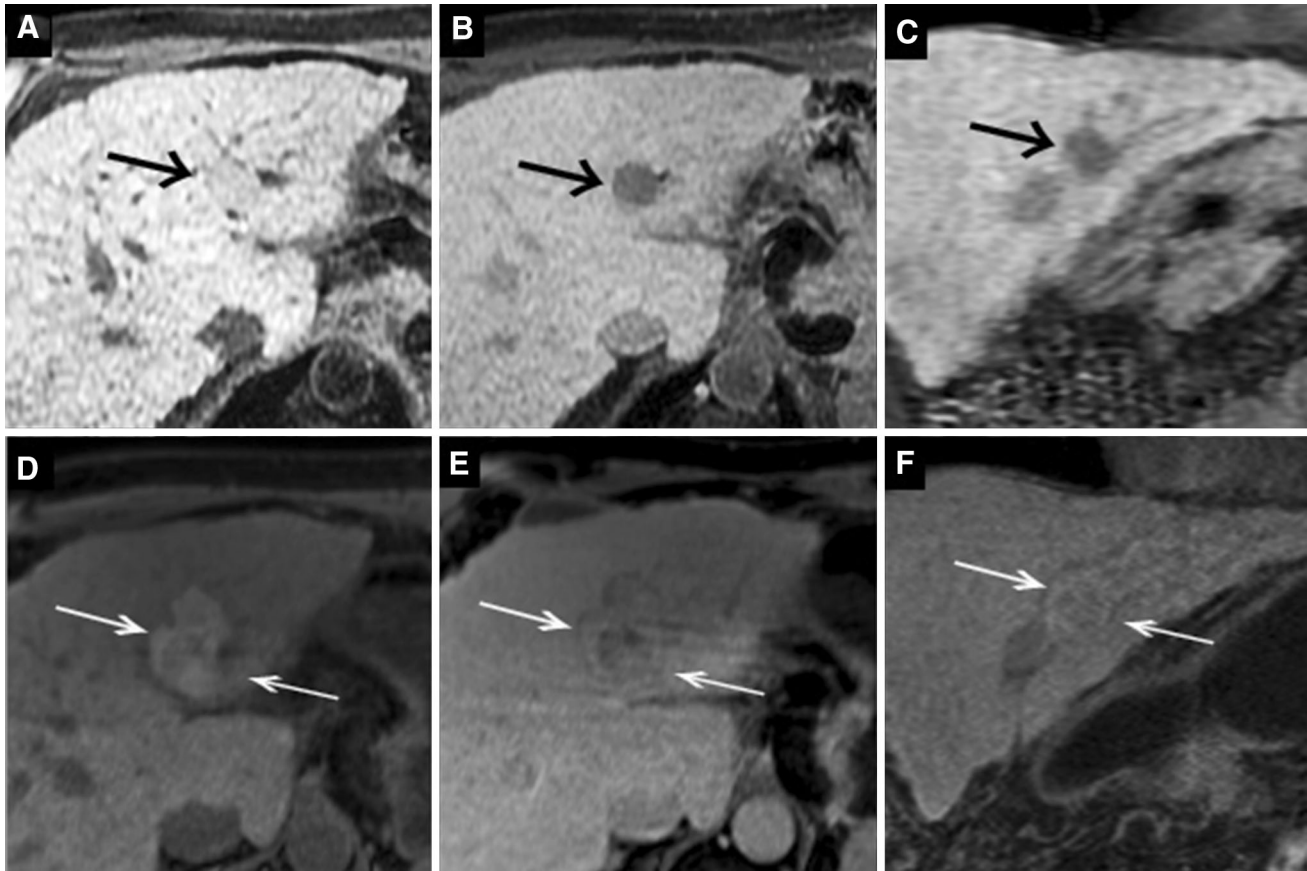


Fig. 6. Images in a 69-year-old man with moderately differentiated hepatocellular carcinoma. At preablation MR imaging, the axial unenhanced T1-weighted image (**A**) shows an isointense tumor (*black arrow*), and axial (**B**) and coronal (**C**) hepatobiliary phase images show a hypointense tumor (*black arrows*). Tumor size is 18 mm, and TLCR on axial unenhanced T1-weighted and HBP imaging are 0.21 and 0.84. After radiofrequency ablation for the tumor, axial unenhanced T1-weighted imaging (**D**) shows a central hyperintense tumor

and a broad hyperintense ablation margin (*white arrow*). This ablation margin is classified as indefinite. Axial (**E**) and coronal (**F**) hepatobiliary phase images show a central hypointense tumor with a marginal hypointensity band (*white arrows*). Ablation margin and hepatic parenchyma show similar intensity. This ablation margin is classified as visible. Using combined images, the status of the ablation margin is AM plus. During 20 months follow-up, there is no evidence of local tumor progression.

Additionally, regarding creating the SI difference between AM and tumor, it may be necessary to increase the SI of hepatic parenchyma as a background against AM. To increase the SI of the background liver, both HBP and portal venous phase imaging can be options to achieve visualization of AM [16]. The reason why HBP sequence was selected was that portal venous phase images could not be evaluated due to severe motion artifacts without breath-hold. Because HBP series are usually reached within 20 min after the initiation of contrast injection in patients with normal hepatic function and last for at least 60 min [21], this long period allows repeated acquisitions in patients who could not hold their breath, and other images to be obtained in different planes.

In our results, 4 additional hypointense tumors and 6 iso-hyperintense ones were detected during axial HBP, and 10 additional hypointense tumors and 9 iso-hyper-

intense ones were visualized during coronal HBP, compared with axial unenhanced T1w images (Table 3). We believe that the first reason for our results was changing the SI of AM from hyperintensity on unenhanced T1w imaging to intermediate-intensity during HBP. Consequently, not only central iso-hyperintense tumors but also hypointense ones could be visualized. Changing the SI of AM was achieved by changing the relative SI among tumor, AM, and hepatic parenchyma, because Gd-EOB-DTPA exhibits high hepatic uptake and high T1 relaxivity, leading to increasing the SI of hepatic parenchyma [21]. In addition, we speculated that the second reason for our results was an interpretation of marginal hypointense band as a hypointense rim during HBP (Figs. 2, 3), which corresponded to sinusoidal congestion with hemorrhage and subsequent inflammatory change [14]. This finding, which was demonstrated more frequently and clearly during HBP than on unen-

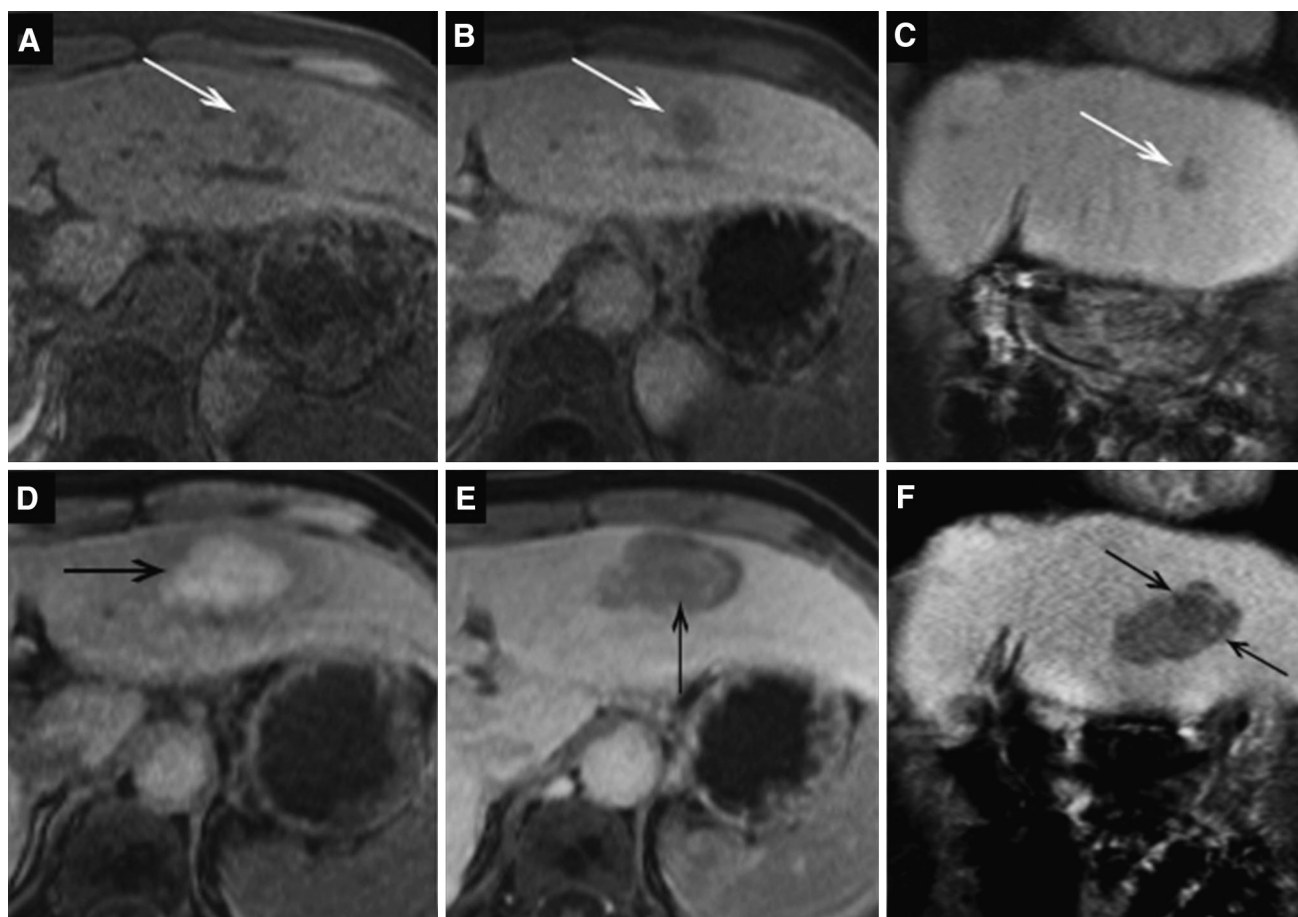


Fig. 7. Images in a 70-year-old woman with moderately differentiated hepatocellular carcinoma. At preablation MR imaging, the axial unenhanced T1-weighted image (**A**) shows a hypointense tumor (*white arrow*), and axial (**B**) and coronal (**C**) hepatobiliary phase images demonstrate a hypointense tumor (*white arrows*). Tumor size is 15 mm, and TLCR on axial unenhanced T1-weighted and HBP imaging are 0.13 and 0.48. After radiofrequency ablation for the tumor, axial unenhanced T1-weighted imaging (**D**) does not distinguish

hyperintensity ablation margin from central hypointensity (*black arrow*). The ablation margin is indefinite. Axial hepatobiliary phase (**E**) shows a hypointensity ablation margin and a vague central tumor (*black arrow*), and coronal hepatobiliary phase image (**F**) shows a central hypointense tumor surrounded by a intermediate-intensity ablation margin (*black arrows*). Using combined images, the status of the ablation margin is AM plus. During 13 months follow-up, there is no evidence of local tumor progression.

hanced T1w images in this study, may be useful to identify the periphery of the ablation zone, even if AM and hepatic parenchyma demonstrate the same signal intensity (Fig. 6), mainly due to liver dysfunction. We considered that the third reason for our results is the use of coronal images, which are taken in a different plane from the axial plane (Fig. 7), and their higher resolution of matrix (320×170 pixels) than in the axial plane (approximately 256×150 pixels or 320×140 pixels). Because FOV of axial images were 38–44 cm, the same as that of coronal images, spatial resolution of the coronal images were higher than axial images. Indeed, some AMs were better seen on unenhanced T1w imaging than HBP, and others were vice versa. Furthermore, the coronal HBP images do not visualize the anterior and posterior edges of the tumor and AMs, axial HBP images might not visualize the cranial and caudal portions of the tumor

and AMs (Fig. 6). We speculated that although some tumors and AMs were only partially visualized in individual sequences, collapsed tumors and ill-defined AMs could be identified using complementarily 2 dimension (Figs. 7, 8). This increased reader confidence when reviewing all 3 sequences. However, coronal unenhanced T1w imaging was not scanned, and thus, it was necessary to compare coronal unenhanced T1w imaging to axial unenhanced T1w with the same resolution to reach a conclusion.

Regarding the relationship between AM visibility and outcome during the follow-up period, combined images were superior to axial unenhanced T1w imaging in both stable and recurrence groups. We consider correlating this with recurrence data to show higher utility of combined images in predicting recurrence based on AM zero or AM minus status.

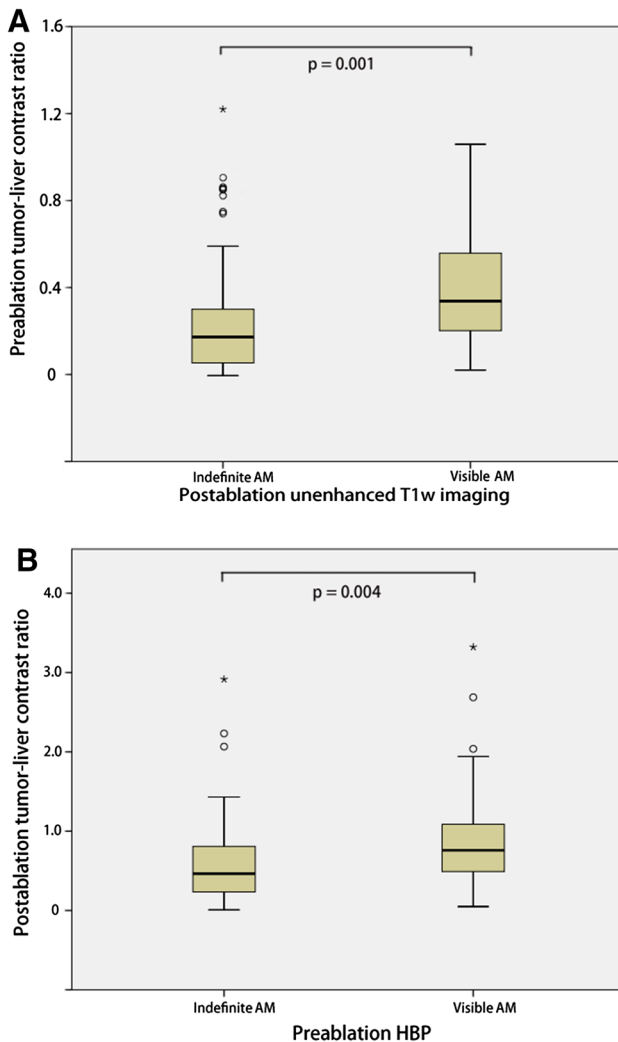


Fig. 8. **A** Comparison of the preablation tumor-liver contrast ratio (TLCR) between two groups with visible and indefinite ablative margin (AM) on postablation axial unenhanced T1w imaging. In the box-and-whisker plots, TLCR in visible AM (0.4 ± 0.2) was a significantly higher ($p = 0.001$) than that (0.2 ± 0.3) in indefinite AM. In *boxes*, *upper* and *lower* margin and *middle horizontal lines* represent upper quartiles (UQs), lower quartiles (LQs), and medians of data, respectively. *Upper* and *lower* ends of *vertical lines* and *circles* represent *upper extremes* [$UQ + 1.56(\text{interquartile range})$], *lower extremes* [$LQ - 1.56(\text{interquartile range})$], and *outliers* of data, respectively. **Fig 8B** Comparison of preablation tumor-liver contrast ratio (TLCR) between two groups with visible and indefinite ablative margin (AM) during postablation axial HBP sequence. In the box-and-whisker plots, TLCR in visible AM (0.9 ± 0.6) was a significantly higher ($p = 0.004$) than that (0.6 ± 0.5) in indefinite AM. In *boxes*, *upper*, and *lower* margin and *middle horizontal lines* represent upper quartiles (UQs), lower quartiles (LQs), and medians of data, respectively. *Upper* and *lower* ends of *vertical lines* and *circles* represent *upper extremes* [$UQ + 1.56(\text{interquartile range})$], *lower extremes* [$LQ - 1.56(\text{interquartile range})$], and *outliers* of data, respectively.

There are several limitations in the present study. First, this was a retrospective study. Therefore, further studies are required to validate the present results in a prospective trial. Second, we did not assess the signal intensity of T2w images and dynamic phases from arterial to late phases. Residual tumor tissue manifests itself as nodular or crescent areas that maintain the signal intensity characteristics displayed on preablation imaging [4, 22]. It is known that, because the ablated zone has a smooth internal contour and displays negligible enhancement after contrast administration, non-circumscribed nodular, or irregular enhancement (wash-in on the arterial phase and washout on the portal venous or late phase) in combination with moderate hyperintensity on T2w images may represent residual and recurrent tumor tissue [2, 22]. Thus, it is difficult to define viable residual tumors as only hypointensity during HBP because approximately 10% of HCCs show iso-hyperintensity during HBP, which can be attributed to the presence of organic anion transporting polypeptide 8 [23]. Third, there were only 21 (15.2%) of 138 HCCs with histological proof of AM and tumor as complete necrosis at transplantation. The other 117 (84.8%) HCCs were diagnosed by follow-up examinations. However, qualitative evaluation of AM in our study may be useful because the incidence of residual tumor and LTP correlated with the AM status by visual assessment as shown in Table 5. Fourth, the follow-up period was 6 months. It is necessary to have a longer follow-up to detect LTP. In addition, intra-observer assessment was not performed, and then there is the question of the reproducibility.

In conclusion, HBP sequence might have higher feasibility to distinguish AM from tumor than axial unenhanced T1w imaging 24 h after thermal ablation. Because different resolutions between axial and coronal images were a major limitation in this study, it is necessary to compare coronal unenhanced T1w imaging to axial unenhanced T1w imaging with the same resolution. The preablation TLCR value in visible AM was higher than that in indefinite AM on both unenhanced T1w and HBP images.

Compliance with ethical standards

Conflict of Interest Nobuyuki Takeyama declares that he has no conflict of interest. Sirachat Vidhyarkorn declares that she has no conflict of interest. Dong Jin Chung declares that he has no conflict of interest. Surachate Siripongsakun declares that he has no conflict of interest. Author B declares that he has no conflict of interest. Hyun J. Kim declares that she has no conflict of interest. David S.K. Lu, declares that he has no conflict of interest. Steven S. Raman declares that he has no conflict of interest.

Ethical approval All procedures performed in studies involving human participants were in accordance with the ethical standards of the institutional and/or national research committee and with the 1964 Helsinki declaration and its later amendments or comparable ethical standards.

References

1. Sainani NI, Gervais DA, Mueller PR, Arellano RS (2013) Imaging after percutaneous radiofrequency ablation of hepatic tumors: Part 1, normal findings. *AJR Am J Roentgenol* 200:184–193
2. Sainani NI, Gervais DA, Mueller PR, Arellano RS (2013) Imaging after percutaneous radiofrequency ablation of hepatic tumors: Part 2, abnormal findings. *AJR Am J Roentgenol* 200:194–204
3. Kierans AS, Elazzazi M, Braga L, et al. (2010) Thermoablative treatments for malignant liver lesions: 10-year experience of MRI appearances of treatment response. *AJR Am J Roentgenol* 194:523–529
4. Kei SK, Rhim H, Choi D, et al. (2008) Local tumor progression after radiofrequency ablation of liver tumors: analysis of morphologic pattern and site of recurrence. *AJR Am J Roentgenol* 190:1544–1551
5. Mulier S, Ni Y, Jamart J, et al. (2005) Local recurrence after hepatic radiofrequency coagulation: multivariate meta-analysis and review of contributing factors. *Ann Surg* 242:158–171
6. Ng KK, Poon RT, Lo CM, et al. (2008) Analysis of recurrence pattern and its influence on survival outcome after radiofrequency ablation of hepatocellular carcinoma. *Gastrointest Surg* 12:183–191
7. Goldberg SN, Gazelle GS, Mueller PR (2000) Thermal ablation therapy for focal malignancy: a unified approach to underlying principles, techniques, and diagnostic imaging guidance. *AJR Am J Roentgenol* 174:323–331
8. Kim YS, Rhim H, Lim HK, et al. (2001) Coagulation necrosis induced by radiofrequency ablation in the liver: histopathologic and radiologic review of usual to extremely rare changes. *Radiographics* 31:377–390
9. Lee JD, Lee JM, Kim SW, Kim CS, Mun WS (2001) MR imaging-histopathological correlation of radiofrequency thermal ablation in a rabbit liver model: observation during acute and chronic stages. *Korean J Radiol* 2:151–158
10. Onishi H, Matsushita M, Murakami T, et al. (2004) MR appearances of radiofrequency thermal ablation region: histopathologic correlation with dog liver models and an autopsy case. *Acad Radiol* 11:1180–1189
11. Hyodoh H, Furuse M, Kawamoto C, et al. (2000) Microwave coagulation therapy: ex vivo comparison of MR imaging and histopathology. *J Magn Reson Imaging* 11:168–173
12. Clasen S, Pereira PL (2008) Magnetic resonance guidance for radiofrequency ablation of liver tumors. *J Magn Reson Imaging* 27:421–433
13. Rempp H, Clasen S, Pereira PL (2012) Image-based monitoring of magnetic resonance-guided thermoablative therapies for liver tumors. *Cardiovasc Interv Radiol* 35:1281–1294
14. Khankan A, Murakami T, Onishi H, et al. (2008) Hepatocellular carcinoma treated with radio frequency ablation: an early evaluation with magnetic resonance imaging. *J Magn Reson Imaging* 27:546–551
15. Koda M, Tokunaga S, Miyoshi K, et al. (2012) Assessment of ablative margin by unenhanced magnetic resonance imaging after radiofrequency ablation for hepatocellular carcinoma. *Eur J Radiol* 81:2730–2736
16. Yoon JH, Lee EJ, Cha SS, et al. (2010) Comparison of gadoteric acid-enhanced MR imaging versus four-phase multi-detector row computed tomography in assessing tumor regression after radiofrequency ablation in subjects with hepatocellular carcinomas. *J Vasc Interv Radiol* 21:348–356
17. American College of Radiology website. (2014) Liver imaging reporting and data system. www.acr.org/Quality-Safety/Resources/LIRADS. Accessed March 21.
18. Mori K, Fukuda K, Asaoka H, et al. (2009) Radiofrequency ablation of the liver: determination of ablative margin at MR imaging with impaired clearance of ferucarbotran-feasibility study. *Radiology* 251:557–565
19. Ringe KI, Wacker F, Raatschen HJ (2015) Is there a need for MRI within 24 hours after CT-guided percutaneous thermoablation of the liver? *Acta Radiol* 56:10–17
20. Braga L, Semelka RC (2005) Magnetic resonance imaging features of focal liver lesions after intervention. *Top Magn Reson Imaging* 16:99–106
21. Ringe KI, Husarik DB, Sirlin CB, Merkle EM (2010) Gadoteric acid-enhanced MRI of the liver: Part 1, protocol optimization and lesion appearance in the noncirrhotic liver. *AJR Am J Roentgenol* 195:13–28
22. Clasen S, Boss A, Schmidt D, et al. (2006) Magnetic resonance imaging for hepatic radiofrequency ablation. *Eur J Radiol* 59:140–148
23. Zech CJ, Bartolozzi C, Bioulac-Sage P, et al. (2013) Consensus report of the fifth international forum for liver MRI. *AJR Am J Roentgenol* 201:97–107